Chapter 5
Mixed Thermal Boundary Condition Effects on Non-Darcian Model

Hajar Lagziri and Hanae EL Fakiri

Abstract The chapter tackles the influence of inertia and thermal boundary effects on thermoconvective instability in the configuration of non Darcian model by using a root-finding algorithm of the shooting method. The set-up assumed here is a homogeneous horizontal isotropic saturated porous layer sandwiched between two rigid impermeable walls where the upper layer is maintained at the isothermal condition and the lower one at the Robin-type thermal boundary condition whose expression is modelled as newton's cooling law equation. The thermal non-equilibrium regime (LTNE) is applicable by imposing different temperatures between Newtonian fluid and the solid medium. The LTNE existence creates two independent Biot numbers besides other non-dimensionless parameters. Normal modes technique is adopted here by applying small disturbances to the dimensionless governing equations. Overall, the finding results will discuss at which instability takes place with respect to different physical numbers.

Keywords Brinkman model · Biot number · Thermal non-equilibrium · Linear stability analysis

5.1 Introduction

In the industrial sector, materials with higher porosity such as metal foams are often used to enhance heat exchange between two bodies or structures. Furthermore, their large surface area and lightweight make them good candidates for recycling energy efficiently. In this case, the usual Darcy's law becomes no longer suitable for describing fluid motion and, it is necessary to adopt the Brinkman-Darcy model instead (Nield 2017; Dubey and Murthy 2019; Bouachir et al. 20121; Caprone and Rionero 2016).

H. Lagziri (✉) · H. EL Fakiri
Department of Physics, Abdelmalek Essaadi University, Quartier M'haneche II, avenue Palestine, 93000 Tetouan, Morocco
e-mail: lagziri-hajar7@hotmail.fr

J. Mabrouki et al. (eds.), *Advanced Technology for Smart Environment and Energy*, Environmental Science and Engineering,
https://doi.org/10.1007/978-3-031-25662-2_5

Moreover, many man-made materials like porous media have anisotropic mechanical and thermal properties. Because of that, thermal instability can be managed by the permeability and thermal conductivity of the medium (Storesletten and Rees 1997; Tyvand and Storesletten 2015; Govender and Vadasz 2007; Mahjoob and Vafai 2008). Rotation also plays a vital role in thermoconvective instability, for example rotating machinery and centrifugal filtration processes. A reference to a rotating frame must be established to investigate the situations in which the solid matrix rotates (Vadasz 2016, 2019; Govender and Vadasz 2007). Otherwise, thermal instability or convection in the subjects of rotating solid matrix, free and forced convection layer with cavities, a non-Darcian model with open boundaries or saturating Oldroyd-B fluid are ones of the several papers that deal with the convection phenomenon (Malashetty et al. 2006; Shivakumara et al. 2006; Rees 2002; Baytas 2004; Saeid 2004). Most papers in the last decade are predicated on the idea that the Newtonian fluid phase and the solid medium are everywhere under the same temperature, which is known as the thermal equilibrium regime (LTE). However, this assumption becomes inadequate for many real-world applications, especially when high-speed flows or significant temperature gradients between both phases are present (Fathi-Kelestani et al. 2020; Gandomkar and Gray 2018; Lagziri and Bezzazi 2019; Barletta 2019). In such cases, it is necessary to consider a two-field energy equation model to represent each phase separately, and this emerges as a virtue of no thermal equilibrium behaviour (LTNE). In addition, it is anticipated that the model of LTNE will have an important role in future technology consisting of porous media such as computer chips, tube refrigerators, heat exchangers and others (Mahjoob and Vafai 2008; Pulvirenti et al. 2020).

The chapter studies the emergence of thermal instability cells in a non-Darcian flow using mixed thermal boundary conditions and a thermal non-equilibrium regime. The influence of these two features on instability behaviour is investigated in detail.

5.2 Mathematical Modeling

A homogeneous fluid-saturated porous layer sandwiched between two rigid impermeable walls is shown in Fig. 5.1. An external heat source is imposed at the lower boundary with two different external heat transfer coefficients h_f and h_s. In other words, Robin's thermal boundary conditions are considered. On the other hand, uniform perfect conducting temperature T_1 is applied at the upper layer. The local thermal nonequilibrium model and linear Oberbeck Boussinesq approximation are both pertinent here. The Brinkman-Darcy equation describes the saturating non-Darcian flow in a solid matrix. Following these descriptions the Mathematical equations of the problem are

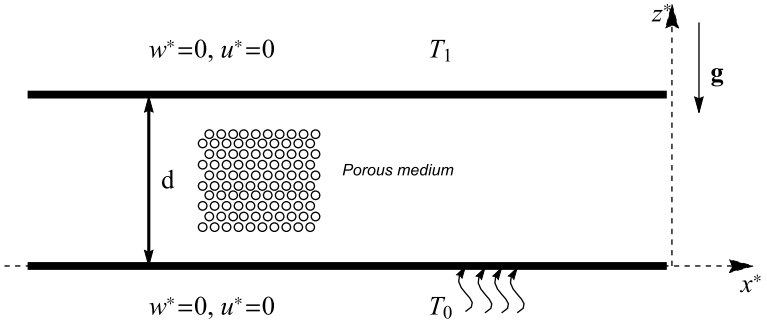

Fig. 5.1 Sketch of Brinkman model with mixed thermal boundary conditions

$$\nabla^* \cdot \vec{u^*} = 0, \tag{5.1a}$$

$$\rho\left[\frac{1}{\phi}\frac{\partial \vec{u^*}}{\partial t^*} + \frac{1}{\phi^2}(\vec{u^*}\cdot\nabla^*)\vec{u^*}\right] + \frac{\mu}{K}\vec{u^*} = -\nabla^* P^* + \mu'\nabla^{*2}\vec{u^*} + \rho_f \beta g(T_f^* - T_0)\vec{ez}, \tag{5.1b}$$

$$(1-\phi)(\rho C)_s \frac{\partial T_s^*}{\partial t^*} = (1-\phi)\alpha_s \nabla^{*2} T_s^* + h(T_f^* - T_s^*), \tag{5.1c}$$

$$\phi(\rho C)_f \frac{\partial T_f^*}{\partial t^*} + (\rho C)_f(\vec{u^*}\cdot\nabla^*)T_f^* = \phi\alpha_f \nabla^{*2} T_f^* - h(T_f^* - T_s^*). \tag{5.1d}$$

The temperature and velocity conditions suggested at the boundary are

$$z^* = d: \quad w^* = 0, u^* = 0, \quad T_s^* = T_f^* = T_1. \tag{5.2a}$$

$$z^\star = 0: \quad w^* = 0, u^* = 0, \quad k_s \frac{\partial T_s^*}{\partial z^*} = h_s(T_s^* - T_0), \quad k_f \frac{\partial T_f^*}{\partial z^*} = h_f(T_f^* - T_0) \tag{5.2b}$$

The superscript of the star notation refers to dimensional variables. The vector $\vec{u}$ means the velocity field. Otherwise, we have also other physical properties such as the thermal diffusivity α with $[m^2/s]$, the effective viscosity μ' with $[N.s/m^2]$, the dynamic viscosity of the fluid μ with $[N.s/m^2]$, the coefficient of thermal expansion β the pressure P, the temperature at the lower wall T_0, the reference density ρ with $[Kg/m^3]$, the inter-phase volumetric heat transfer coefficient h with $[W/(m^3K)]$, the heat capacity per unit of mass C with $[J/(KgK)]$, the porosity ϕ, the time t with $[s]$, the thickness of the layer d with $[m]$, the thermal conductivity k with $[W/(mK)]$, the superficial heat transfer coefficient between both phases $h_{s,f}$ with $[W/(m^2K)]$ and the permeability K with $[m^2]$.

The dimensionless expression of the governing equations is,

$$\begin{aligned} \nabla \times (D^{-1}\vec{u} - \nabla^2\vec{u}) &= RD^{-1}[\nabla \times T_f]\vec{ez}, \\ \lambda\frac{\partial T_s}{\partial t} &= \nabla^2 T_s + \gamma H(T_f - T_s), \\ \frac{\partial T_f}{\partial t} + \vec{u}\cdot\nabla T_f &= \nabla^2 T_f + H(T_s - T_f), \end{aligned} \tag{5.3}$$

We get the resulting boundary conditions as

$$\begin{aligned} z = 1: \quad & w = 0, \quad u = 0, \quad T_s = T_f = 0, \\ z = 0: \quad & w = 0, \quad u = 0, \quad \frac{\partial T_s}{\partial z} = B_s(T_s - 1), \quad \frac{\partial T_f}{\partial z} = B_f(T_f - 1). \end{aligned} \tag{5.4}$$

The notations "s" and "f" signify the saturating Newtonian fluid phase and solid structure. The dimensionless forms of R and H mean the modified thermal Rayleigh number and the inter-heat transfer coefficient while B_s and B_f describe the Biot number of the solid matrix and fluid phase. Besides, we have γ and D whose physical meanings are the thermal conductivity ratio and the Darcy number respectively.

The dimensionless parameters that emerge in (5.3) and (5.4) are:

$$\begin{aligned} \lambda = \frac{\alpha_f}{\alpha_s}, \quad k_m = (1-\phi)k_s + \phi k_f, \quad \gamma = \frac{\phi k_f}{(1-\phi)k_s}, \\ H = \frac{hd^2}{\phi k_f}, \quad B_{s,f} = \frac{h_{s,f}d}{k_{s,f}}, \quad \alpha_f = \frac{k_f}{(\rho C)_f}, \quad \alpha_m = \frac{k_m}{(\rho C)_f}, \\ D = \frac{\mu' K}{\mu d^2}, \quad R = \frac{\rho_f \beta \Delta T g K d}{\nu k_f \phi}, \quad \Delta T = \frac{\phi(T_1 - T_0)d}{k_m}. \end{aligned} \tag{5.5}$$

where the rescaling variables applicable in the set of governing equations are,

$$\nabla^* \to \nabla\frac{1}{d}, \quad t^* \to \frac{d^2}{\alpha_f}, \quad \vec{u^*} \to \vec{u}\frac{\phi\alpha_f}{d}, \quad T^*_{s,f} \to T_0 + T_{s,f}\Delta T. \tag{5.6}$$

5.3 Basic Profile

We consider a motionless flow whose basic state is

$$\vec{u}_b = 0, \quad T_{f,b} = T_{fb}(z), \quad T_{s,b} = T_{sb}(z). \tag{5.7}$$

We have used "b" as a symbol of the basic flow.

5.3.1 Linear Stability Analysis

Let us disturb the basic flow by writing that

$$\begin{aligned} \vec{u} &= \vec{u}_b + \epsilon\vec{U}, \\ T_{fs} &= T_{sf,b}(z) + \epsilon\theta_{s,f}. \end{aligned} \tag{5.8}$$

We are concerned only with the first-order terms of disturbances, therefore, the linearized form of the equations is

$$\nabla \times (D^{-1}\vec{U} - \nabla^2\vec{U}) = RD^{-1}[\nabla \times \theta_f]\vec{ez} = 0, \tag{5.9a}$$

$$\theta_s{}'' - a^2\theta_s + \gamma H(\theta_f - \theta_s) = 0, \tag{5.9b}$$

$$\theta_f{}'' - a^2\theta_f + H(\theta_s - \theta_f) - aT'_{f,b}\vec{U} = 0, \tag{5.9c}$$

$$z = 1: \quad W = 0, \quad U = 0, \quad \theta_s = \theta_f = 0. \tag{5.9d}$$

$$z = 0: \quad W = 0, \quad U = 0, \quad \theta_s{}' - \theta_s B_s = 0, \quad \theta_f{}' - \theta_f B_f = 0, \tag{5.9e}$$

Now we apply the normal modes method by defining the functions as

$$\begin{aligned} \vec{U}(x,z,t) &= \Re\{i\hat{\vec{U}}(z)e^{i(ax-\omega t)}\}, \\ \theta_f(x,z,t) &= \Re\{\theta(z)e^{i(ax-\omega t)}\}, \\ \theta_s(x,z,t) &= \Re\{\varphi(z)e^{i(ax-\omega t)}\} \end{aligned} \tag{5.10}$$

Hence the symbols of $\hat{\vec{U}}$, θ and φ are used to describe the perturbed functions with respect to z. The wave number is defined by the symbol a while the growth rate and the angular frequency are noted with ω_r and ω_i respectively. The complex parameter ω is defined as the sum of the imaginary and real parts.

In the meantime, the velocity components can be expressed in the stream functions as,

$$\hat{U} = \frac{\partial\psi}{\partial z}, \quad \hat{W} = -\frac{\partial\psi}{\partial x}. \tag{5.11}$$

Otherwise, the definition of T'_{fb} is

$$T'_{fb} = \frac{-B_f B_s(\gamma+1)\sinh(\Omega) + (-\Omega)(B_f\gamma + B_s)\cosh(\Omega) + (B_s - B_f)\Omega\cosh(\Omega z)}{(B_f(B_s\gamma + B_s + 1) + B_s\gamma)\sinh(\Omega) + \Omega(B_f\gamma + B_s + \gamma + 1)\cosh(\Omega)}. \tag{5.12}$$

With $\Omega = \sqrt{(1+\gamma)H}$.

By substituting (5.10) and (5.11) into (5.13) the set of equations become,

$$-\psi'''' + (2a^2 + D^{-1})\psi'' - a^2(a^2 + D^{-1})\psi + aD^{-1}R\theta = 0, \tag{5.13a}$$

$$\varphi'' - a^2\varphi + \gamma H(\theta - \varphi) = 0, \tag{5.13b}$$

$$\theta'' - a^2\theta + H(\varphi - \theta) - aT'_{f,b}\psi = 0, \tag{5.13c}$$

$$z = 1: \quad W = 0, \quad U = 0, \quad \varphi = \theta = 0. \tag{5.13d}$$

$$z = 0: \quad W = 0, \quad U = 0, \quad \varphi' - \varphi B_s = 0, \quad \theta' - \theta B_f = 0, \tag{5.13e}$$

As our motivation is to seek the marginal curves, the imaginary part of ω has to be neglected. Meanwhile, the principle of exchange of instabilities is achieved numerically thus we can eliminate both parts of ω and write (5.13).

5.4 Numerical Solutions

The numerical method adopted for dealing with (5.13) is the shooting method and Range-Kutta solver. In general, this latter required the definition of extra boundary conditions as a first step to manage (5.13) in the form of an initial value problem. Thus, we can add

$$\psi''(0) = \zeta_1, \quad \psi'''(0) = \zeta_2, \quad \varphi(0) = \zeta_3, \quad \theta(0) = 1. \tag{5.14}$$

The condition noted by $\theta(0) = 1$ is included as a virtue of the homogeneity in the governing equations. The parameters of ζ_1, ζ_2 and ζ_3 are considered as unknowns with real values. The next step here is to define these unknown constants together with R for any given value of H, γ, a, D, B_s and B_f through the use of the shooting method and boundary conditions of the upper wall. The shooting method consists in employing the root-finding algorithm in Mathematica 10 to determine the value pair of (R_c, a_c).

5.5 Discussion and Results

Table 5.1 exhibits the critical values of the modified Rayleigh number and wave number for different values of B_s, B_f and H in the cases where $D = 0.01$ and $D = 0.1$. Overall, we note that the Darcy number consists in having the viscous diffusion at the region nearer to the boundary layers. In other words, as much as the viscous effects decrease the fluid can flow and move more rapidly and easily without resistance, thereby the onset of convection can be yielded at a small critical Rayleigh number. Besides, we mention the values of $H = 10$ and $H = 0.1$ as the two approaches of the thermal equilibrium and non-equilibrium one. A small value

Table 5.1 Critical values of R_c and a_c for fixed $\gamma = 1$ and variable values of H, B_s, B_f and D

$B_s = 10$, $D = 0.01$ and $H = 0.1$			$B_s = 10$, $D = 0.01$ and $H = 10$		
B_f	a_c	R_c	B_f	a_c	R_c
10^{-2}	2.511038	1079.598493	10^{-2}	3.104816	112.986416
10^{-1}	2.558604	390.796352	10^{-1}	3.115111	111.056979
10^{0}	2.771452	97.466144	10^{0}	3.192665	99.369782
10^{1}	3.123249	62.807080	10^{1}	3.380695	83.971631
10^{2}	3.224927	60.824797	10^{2}	3.468684	80.081593
$B_f = 10$, $D = 0.01$ and $H = 0.1$			$B_f = 10$, $D = 0.01$ and $H = 10$		
B_s	a_c	R_c	B_s	a_c	R_c
10^{-2}	3.123464	63.182457	10^{-2}	3.324845	93.982412
10^{-1}	3.123442	63.149355	10^{-1}	3.326237	93.474899
10^{0}	3.123335	62.980012	10^{0}	3.338512	90.032296
10^{2}	3.123237	62.772448	10^{2}	3.402791	82.268740
$B_s = B_f$, $D = 0.01$ and $H = 0.1$			$B_s = B_f$, $D = 0.01$ and $H = 10$		
10^{-2}	2.536034	4623.735494	10^{-2}	2.912826	6722.170507
10^{-1}	2.567577	508.663163	10^{-1}	2.936807	736.272960
10^{0}	2.772213	99.083327	10^{0}	3.095060	139.361525
10^{2}	3.224927	60.824797	10^{2}	3.468684	80.081593
$B_s = 10$, $D = 0.1$ and $H = 0.1$			$B_s = 10$, $D = 0.1$ and $H = 10$		
B_f	a_c	R_c	B_f	a_c	R_c
10^{-2}	2.547663	3916.656653	10^{-2}	3.049394	406.099765
10^{-1}	2.590804	1409.760163	10^{-1}	3.057606	399.046135
10^{0}	2.771510	349.394966	10^{0}	3.118962	356.437503
10^{1}	3.062273	223.926148	10^{1}	3.265212	300.650240
10^{2}	3.144334	216.690171	10^{2}	3.321342	289.612267
$B_f = 10$, $D = 0.1$ and $H = 0.1$			$B_f = 10$, $D = 0.1$ and $H = 10$		
B_s	a_c	R_c	B_s	a_c	R_c
10^{-2}	3.062456	225.261482	10^{-2}	3.217395	336.521693
10^{-1}	3.062437	225.143664	10^{-1}	3.218693	334.689564
10^{0}	3.062348	224.541123	10^{0}	3.229690	322.297643
10^{2}	3.062263	223.803036	10^{2}	3.283231	294.616629
$B_s = B_f$, $D = 0.1$ and $H = 0.1$			$B_s = B_f$, $D = 0.1$ and $H = 10$		
B_s	a_c	R_c	B_s	a_c	R_c
10^{-2}	2.572029	16660.158434	10^{-2}	2.893640	24122.803423
10^{-1}	2.598972	1831.364896	10^{-1}	2.912764	2641.510203
10^{0}	2.772161	355.135619	10^{0}	3.039128	499.382360
10^{2}	3.144336	216.633727	10^{2}	3.333511	286.691853

Table 5.2 Comparison of R_c and a_c with others results for the case of $D = 0$ and $\gamma = 1$

Postelnicu results (Postelnicu 2008)			Shivakumara results (Shivakumara et al. 2010)		Present results	
H	R_c	a_c	R_c	a_c	R_c	a_c
10^{-2}	40.020810	3.163	40.2467	3.171	40.1084	3.166
10^{-1}	40.192163	3.169	40.4271	3.178	40.1523	3.171
10^{0}	41.897	3.232	42.1288	3.241	41.3623	3.211
10^{1}	52.991	3.460	53.2635	3.470	52.3608	3.436
10^{2}	73.258	3.293	73.6547	3.303	72.3404	3.270

Table 5.3 Comparison of R_c and a_c with others results for the case of $D = 1$ and $\gamma = 1$

Postelnicu results (Postelnicu 2008)			Shivakumara results (Shivakumara et al. 2010)		Present results	
H	R_c	a_c	R_c	a_c	R_c	a_c
10^{-2}	1753.1005	3.121	1753.1005	3.121	1753.1005	3.1208
10^{-1}	1761.0641	3.126	1761.0641	3.126	1761.0641	3.1256
10^{0}	1836.336	3.168	1836.3356	3.168	1836.3356	3.1680
10^{1}	2330.852	3.311	2330.2069	3.311	2330.2069	3.3108
10^{2}	3210.852	3.206	3210.8516	3.206	3210.85149	3.2055

of H leads the heat to be poorly exchanged between the two phases whereas for a higher one the ability to heat transfer becomes extremely large. Otherwise, the range assumed for B_s and B_f extends from 10^{-2} to 10^{2} to recover the both thermal conditions of uniform heat flux and perfect conducting temperature. The finding results of Table 5.1 show that the thermal stability increases in the cases where the combined effect of LTNE and fluid inertia is present. In addition, we can notice that even both Biot numbers can have the tendency to emerge stable behaviour.

The results computed by our numerical method in Tables 5.2, 5.3 for the case of $D = 0$ (Darcian flow) and $D = 1$ display a good congruence with those of Postelnicu (2008) and Shivakumara (2010). These two tables confirm that the fluid inertia can retard the fluid motion which decreases later the buoyancy effects in the medium.

The neutral curves evaluated numerically for various values of γ and fixed $D = 0.01$ are drawn in Fig. 5.2. We remind that stability takes place in the regions situated below the concave curves. In fact, all these curves follow the same standard shape of the well-known Benard problem. Therefore, if we look at the behaviour of these curves in the function of γ and both Biot numbers we can notice that stability effects increase with the reduction of these two parameters. The small value of γ manages the heat to be transported only through the solid structure, this in turn slows the onset of convection especially when both phases at the upper layer have no ability to enter

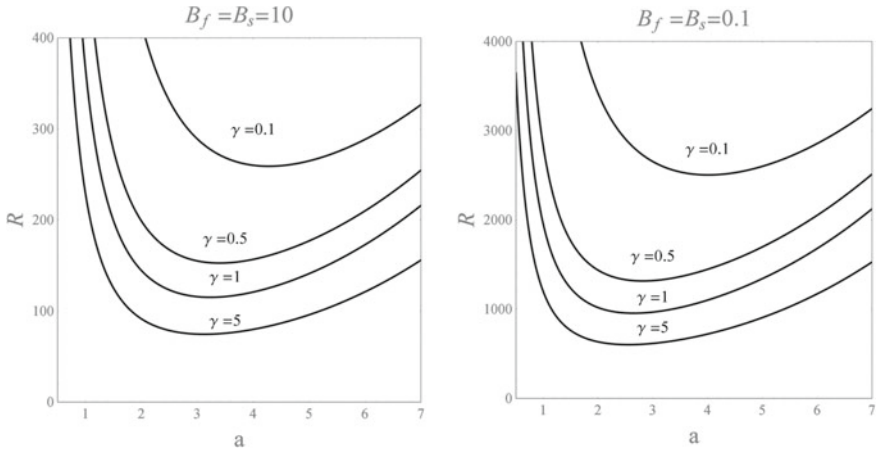

Fig. 5.2 Neutral curves for $H = 100$ and $D = 0.01$

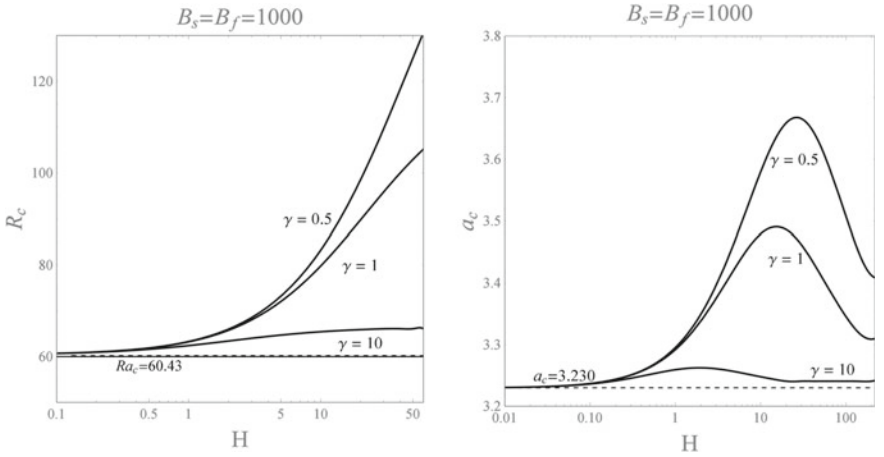

Fig. 5.3 Plots for R_c and a_c versus H with $B_f = B_s = 1000$ and $D = 0.01$

or outer the heat with the external environment. Otherwise, Figs. 5.3, 5.4 display the variation of R_c and a_c with respect to H for $D = 0.01$. The broken lines in both figures describe the critical values at thermal equilibrium. The results extracted from both figures confirm that the stability effects prevail more in the case of uniform heat flux as $R_c = 11427.15$ and $a_c = 2.5$ for $\gamma = 10$.

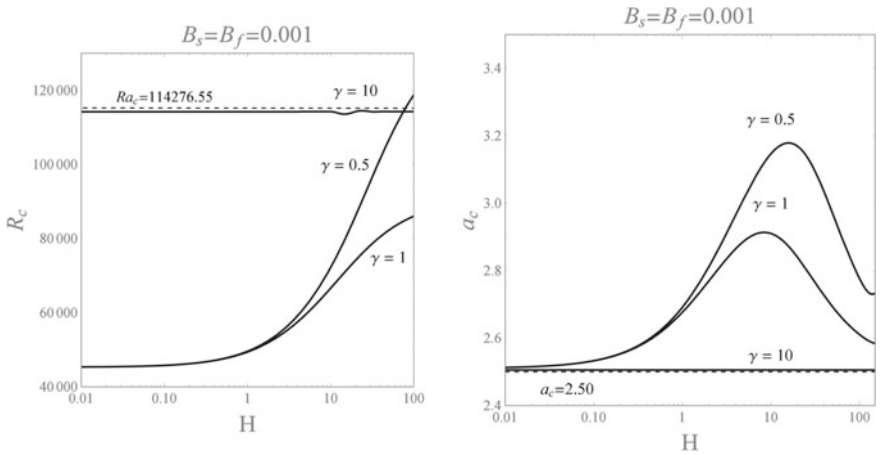

Fig. 5.4 Plots for R_c and a_c versus H with $B_f = B_s = 0.001$ and $D = 0.01$

5.6 Conclusion

The combined effect of non Darcian model and LTNE regime in a porous layer with mixed thermal boundary conditions is investigated in this chapter. The root-finding algorithm of the shooting method and Runge-Kutta solver are considered to solve numerically the eigenvalue problem tackled by linear stability analysis. Briefly, the finding results may be summed up as

- The thermal non-equilibrium (LTNE) regime with weak heat exchange at the upper layer by fluid phase creates more stability than the solid one.
- The growth of Darcy's number hastens the stability as a result of the fluid inertia. In other words, the buoyancy effects become less dominant in front of inertia effects.
- The reduction in both Biot numbers brings about stabilizing effects in the medium either in LTE or LTNE model.

Acknowledgements This research was not funded by any grant.

References

AL-Sumaily Gazy F, Al Ezzi A, Dhahad Hayder A, Thompson Mark C, Yusaf T (2021) Legitimacy of the local thermal equilibrium hypothesis in porous media: a comprehensive review. J Eng (14):2–47

Barletta A, Rees DAS on the onset of convection in a highly permeable vertical porous layer with open boundaries. AIP Phys Fluids 31:112 (2019)

Baytas AC (2004) Thermal non-equilibrium free convection in a cavity using the non-Darcy porous medium. In: Ingham DB (2004)

Bouachir A, Mamon M, Rebhi R, Benissaadi S (2021) Linear and nonlinear stability analyses of double-diffusive convection in a vertical brinkman porous enclosure under Soret and Dufour effects. Fluids 6:292

Caprone F, Rionero S (2016) Brinkman viscosity action in porous MHD convection. Int J Non-Linear Mech 85:109–117

Dubey R, Murthy PVSN (2019) The onset of double-diffusive convection in a Brinkman porous layer with convective thermal boundary conditions. AIP Adv 9:045322

Fathi-Kelestani A, Nazari M, Mahmoudi Y (2020) Pulsating flow in a channel filled with a porous medium under local thermal non-equilibrium condition: an exact solution. J Therm Analy Calori 145:2753–2775

Gandomkar A, Gray KE (2018) Local thermal non-equilibrium in porous medium with heat conduction. Int J Heat Mass Trans 124:1212–1216

Govender S, Vadasz P (2007) The effect of mechanical and thermal anisotropy on the stability of gravity-driven convection in rotating porous media in the presence of thermal non-equilibrium. Transp Porous Media 69:55–66

Lagziri H, Bezzazi M (2019) Robin boundary effects in the Darcy-Rayleigh problem with local thermal non-equilibrium model. Trans Porous Media 129:701–720

Mahjoob S, Vafai K (2008) A synthesis of fluid and thermal transport model for metal foam heat exchangers. Int J Heat Mass Trans 51:3701–3711

Malashetty MS, Shivakumara IS, Kulkarni S (2005) The onset of convection in an anisotropic porous layer using a thermal non-equilibrium model. Transp Porous Media 60:199–215

Malashetty MS, Shivakumara IS, Kulkarni S, Swamy M (2006) Convective instability of Oldroyd-Bfluid saturated porous layer heated from below using a thermal non-equilibrium model. Transp Porous Media 64:123–139

Nield AD, Bejan A (2017) Convection in porous media, 5th edn. Springer, New York

Postelnicu A (2008) The onset of Darcy-Brinkman convection using a thermal non-equilibrium model—Part II. Int J Thermal Sci 47:1587–1594

Pulvirenti B, Celli M, Barletta A (2020) Flow and convection in metal foams: a survey and new CFD results. Fluids 5:155–225

Rees DAS, Pop I (2002) Vertical free convective boundary layer flow in a porous medium using a thermal non -equilibrium model: elliptic effects. J Appl Math Phys 53:1–12

Saeid NH (2004) Analysis of mixed convection in a vertical porous layer using the non-equilibrium model. Int J Heat Mass Trans 47:5619–5627

Shivakumara IS, Malashetty MS, Chavaraddi KB (2006) Onset of convection in a viscoelastic fluid saturated sparsely packed in a porous layer using a thermal non-equilibrium model. Can J Phys 84:973–990

Shivakumara IS, Mamatha AL, Ravisha M (2010) Boundary and thermal non-equilibrium effects on the onset of Darcy-Brinkman convection in a porous layer. J Eng Math 47:317–328

Storesletten L, Rees DAS (1997) An analytical study of free convective boundary layer flow in porous media: the effect of anisotropic diffusivity. Transp Porous Media 27:289–304

Tyvand PA, Storesletten L (2015) Onset of convection in an anisotropic porous layer with vertical principal axes. Transp Porous Media (10)8:581–593 (2015)

Vadasz P (2019) Instability and convection in rotating porous media. Rev Fluids 4:147 (2019)

Vadasz P (2016) Fluid flow and heat transfer in rotating porous media. Springer, New York